I&EC research
Industrial & Engineering Chemistry Research

pubs.acs.org/IECR

Article

Primary Drying Optimization in Pharmaceutical Freeze-Drying: A Multivial Stochastic Modeling Framework

Gabriele Bano, Riccardo De-Luca, Emanuele Tomba, Agnese Marcelli, Fabrizio Bezzo, and Massimiliano Barolo*

Cite This: *Ind. Eng. Chem. Res.* 2020, 59, 5056−5071

Read Online

ACCESS | Metrics & More | Article Recommendations

ABSTRACT: Primary drying is the most time-consuming and energy-intensive step in pharmaceutical freeze-drying. Minimizing the duration of this stage is of paramount importance to speed up process development and product manufacturing. In this study, we propose a stochastic modeling framework that can help to reach this target. The framework is composed of five sequential steps: model development, sensitivity analysis, model calibration, model validation, and dynamic optimization. Three critical issues are addressed and accounted for in the model structure, namely, (i) the effect of time-varying operating conditions on the process key performance indicators (KPIs); (ii) the dynamic evolution of the water vapor partial pressure inside the drying chamber; and (iii) the impact of drying heterogeneity on the primary drying duration. We cope with the first two issues by introducing macroscopic energy and mass balances within the model formulation. The third issue is addressed by allocating intralot variability as a parametric uncertainty in the model parameter with the strongest sensitivity toward the process KPIs. The proposed stochastic model is calibrated and validated with data generated from industrial experiments. Nonlinear dynamic optimization is then exploited to minimize the duration of primary drying while simultaneously guaranteeing the fulfillment of tight constraints on the product temperature and sublimation rate. Experimental results show a reduction of ∼20% of the primary drying duration with the optimized protocol when compared to standard (i.e., at constant shelf temperature and chamber pressure) protocols, while ensuring the same product quality.

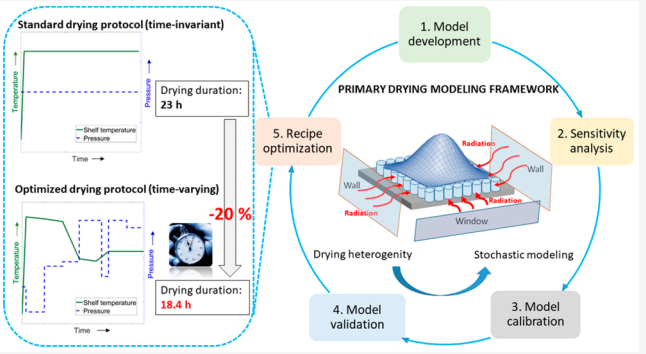

1. INTRODUCTION

Many temperature-sensitive products involved in the biopharmaceutical industry (e.g., enzymes, vaccines, and monoclonal antibodies) exhibit a limited stability if kept in aqueous solution for a long time. A process that can be used to promote long-term stability for these products while avoiding the thermal degradation of their structure is lyophilization (also known as freeze-drying).

Lyophilization is a time-consuming and energy-demanding process that consists of three main steps: freezing, primary drying, and secondary drying. In the first step, the product is frozen at very low temperature (around −50 °C) and most of the water solvent is converted to ice. In the second step, ice is removed from the frozen product by direct sublimation at low temperature (around −20 to −30 °C) and low pressure (around 50−100 mTorr). In the third and last step, the unfrozen water that did not crystallize during freezing and that is bound to the product is desorbed at higher temperature (around 20 to 30 °C).

In most applications, primary drying represents by far the longest as well as the most energy-intensive step of the entire process.[1,2] Therefore, optimizing this step is crucial to reducing the total process duration, thus in turn increasing the process productivity and profitability.

Primary drying optimization consists of identifying the optimal combination of the manipulated inputs, namely, shelf temperature and chamber pressure, that allows sublimation to be completed in all of the vials of the batch in the shortest possible time while fulfilling tight constraints on both product temperature and sublimation rate.[3] The product temperature must not exceed the collapse temperature (for amorphous materials) or the eutectic temperature (for crystalline materials) of the product in order to avoid a loss of pore structure,[4] which compromises the visual appearance of the final product.[5,6] The sublimation rate cannot exceed the maximum capacity of the duct connecting the drying chamber to the condenser in order to

Received: November 21, 2019
Revised: February 14, 2020
Accepted: February 24, 2020
Published: February 24, 2020

https://dx.doi.org/10.1021/acs.iecr.9b06402
Ind. Eng. Chem. Res. 2020, 59, 5056−5071

avoid water vapor accumulation in the chamber, thereby causing a loss of pressure control with potential quality-related and safety-related consequences for the entire lyophilization cycle.[4]

Given these tight constraints, in the industrial practice the operation of the primary drying stage typically results from experience-based, time-consuming experimental campaigns. The resulting recipe (i.e., the combination of shelf temperature and chamber pressure under which the sublimation process is operated) is often very conservative and far from optimal, thus presenting a considerable scope for improvement. Recipe optimization can be achieved if a reliable mathematical model for the process is available, where the model describes in silico the underlying mechanisms relating the operating conditions to the key performance indicators (KPIs), namely, product temperature, sublimation rate, and residual ice content, of primary drying.

Several modeling approaches have been proposed to serve this purpose. These include detailed multidimensional models based on finite-element formulations[7−12] as well as simplified monodimensional models.[1,13−15] Multidimensional models involve a large number of model parameters, and their application for optimization purposes is limited by the high computational cost.[16] On the other side, monodimensional models involve fewer parameters and are computationally cheaper. This simplicity is obtained at the expense of neglecting radial temperature and composition gradients as well as different heat-transfer mechanisms (such as radiation) or the effect of side vials. Typically, the drying recipe is obtained with these models by performing several in silico simulations at constant chamber pressure and constant shelf temperature until a satisfactory profile of the KPIs is obtained. Alternatively, the recipe is obtained by identifying a set of operating conditions (known as the design space of the process) under which satisfactory product quality can be achieved within the given constraints.[17−19]

Although some authors[20−25] have shown the potential of these models for optimization purposes, the contributions presented in the literature so far still suffer from some limitations.

The first limitation is related to the strategy adopted for the offline calibration of the most significant model parameters, namely, the heat- and mass-transfer coefficients. The heat-transfer parameters are typically estimated from gravimetric experiments with pure water[26] or from ad hoc experiments such as the pressure rise test[4,20] (PRT), the Lyobalance,[27] or tunable diode laser absorption spectroscopy[28,29] (TDLAS). The mass-transfer parameters can be estimated with the PRT or TDLAS as well, or they can be inferred from temperature data obtained from single or multiple lyophilization cycles[16] based on the previously estimated values of the heat-transfer parameters. In this last scenario, the estimated values of the mass-transfer parameters directly depend on the accuracy of the estimated values of the heat-transfer parameters. As a result, uncertainty in the latter unavoidably propagates to the former. Moreover, it is well known[26,30] that the vials where temperature probes (e.g., thermocouples) are placed behave differently from non-monitored vials, which on the other hand are much greater in number. The probe, in fact, can act as a nucleation site and typically promotes greater sublimation rates.[26] The estimation of mass-transfer parameters based only on temperature data can therefore compromise the prediction fidelity of the model, potentially affecting its ability to describe the behavior of the majority of the vials inside the drying chamber.

The second limitation of currently available studies is related to the fact that the identification of the optimal recipe for primary drying is typically performed by assuming time-invariant profiles for the manipulated inputs, despite the fact that most industrial equipment (on both the laboratory and manufacturing scales) allows setting time-varying profiles for them. This is due to two main reasons. The first one is that using time-invariant operating conditions is consistent with the experience-based, conservative approach that is typically adopted for primary drying design and optimization in industrial practice. The second reason is that most of the monodimensional models available in the literature approximate the behavior of the process as pseudo-steady-state.[16,31,32] This assumption, however, obviously does not hold true under time-varying operating conditions (e.g., these models cannot be used to describe the product temperature dynamics following a change in the shelf temperature). Limiting the primary drying operation to time-invariant manipulated variable profiles strongly reduces the potential for process improvement.

The third and last limitation is related to the lack of systematic modeling strategies to include intralot drying heterogeneity within a dynamic optimization framework. Vials placed at different locations in the drying chamber exhibit different sublimation rates and product temperature profiles due to different radiation contributions (e.g., from the drying chamber walls) that can impact the overall heat flux supplied to the frozen product.[32] In fact, vials placed in central positions on the shelf (central vials) are only slightly affected by radiation from the chamber walls; therefore, they exhibit smaller sublimation rates and lower product temperatures. These vials are responsible for the overall drying duration. On the other side, vials directly exposed to the chamber walls (edge vials) exhibit greater sublimation rates and higher product temperatures and thus are more vulnerable to constraint violations. A rigorous optimization strategy should simultaneously consider the behavior of central vials (for reducing primary drying duration) and edge vials (for constraint fulfillment) in the modeling framework. However, the studies currently available in the open literature propose only suboptimal solutions to this problem. In fact, the typical approach consists of calibrating different heat-transfer parameters (average estimates obtained from gravimetric experiments) for central and edge vials. Model-based optimization is then carried out by assuming that all of the vials in the batch behave like the central (in most situations) or edge (less often) vials.[21] Clearly, the optimal recipe obtained assuming that all vials in the batch behave like edge vials allows the constraints on product temperature and sublimation rate to be satisfied but provides only suboptimal results in terms of primary drying duration. On the other hand, the assumption that all of the vials in the batch behave like central vials gives optimal results in terms of primary drying duration, but the resulting protocol does not ensure the required quality of the product in the edge vials because of potential constraint violation. The choice of which of the two assumptions should be made is typically performed by comparing the energy savings derived from a shorter drying time with the product waste due to the rejection of edge vials.[19] Therefore, a modeling solution allowing one to avoid this compromise solution would be highly desirable.

This study is intended to give a systematic modeling framework to overcome the above limitations. We address the first and second limitation (model calibration and time-varying operating conditions) by making few simple, yet powerful

https://dx.doi.org/10.1021/acs.iecr.9b06402
Ind. Eng. Chem. Res. 2020, 59, 5056−5071

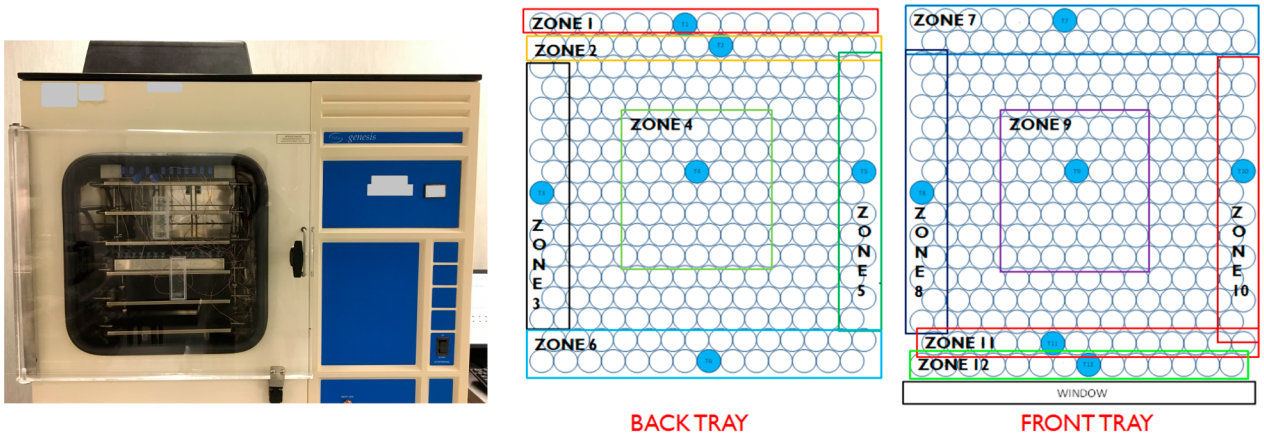

Figure 1. (a) Photograph of a front view of the equipment used in this study. (b) Arrangement of the vials on the shelves. Thermocouples were placed inside the vials shaded in light blue. The rectangular boxes indicate the logic partitioning of vials in thermal zones (due to their different thermal behavior).

modifications to the monodimensional model proposed by Fissore et al.[21] These modifications include (i) the introduction of a dynamic energy balance to capture the effect of time-varying profiles of shelf temperature and chamber pressure on product temperature dynamics; (ii) the introduction of the effects of radiation from the walls and the rails in the energy balance; and (iii) the introduction of a new equation to describe the dynamics of the water partial pressure in the drying chamber. These modifications allow us to keep the model complexity relatively low (few additional parameters to be calibrated) while reaching two targets: obtaining a good model prediction fidelity with time-varying operating conditions and exploiting the information coming from available pressure measurements for the estimation of model parameters. We address the third limitation (drying heterogeneity) first by using global sensitivity analysis (GSA) techniques to identify the model parameter that has the strongest impact on the KPIs and then by introducing a stochastic description of this parameter. We then perform a dynamic optimization of the primary drying duration using rigorous nonlinear programming techniques. We finally test the results of the model-based optimization by experimentation on industrial laboratory-scale equipment.

2. MATERIALS AND METHODS

Although different configurations can be used to carry out freeze-drying, in this study we will refer to a situation where the product is processed inside vials, which are placed over shelves, through which a heating fluid (typically, a silicone oil) flows and supplies the energy required for sublimation. The product is processed inside a high-vacuum drying chamber, which is connected to a condenser (through a duct) that removes the water vapor by sublimation.

2.1. Experimental Setup. The experiments presented in this study were performed on a 5% w/w sucrose solution. The solution was processed in a VirTis Genesis 25EL freeze-dryer (SP Scientific, Stone Ridge, NY, USA) using nonsiliconized 3 [mL] vials filled with 0.6 [mL] of solution. One full shelf out of a total of five was loaded in each experiment (partial loading), as shown in Figure 1a. Two different vial frames were loaded for each shelf. Each frame was surrounded by a metallic rail and contained 238 vials, for a total of 476 vials inside the drying chamber. To account for the different thermal behavior of the vials inside the chamber, each frame was logically partitioned into six different zones, each of which with expected similar thermal behavior. A total of 12 thermal zones were identified. The logic partitioning of the vials is schematically shown in Figure 1b. It can be seen that zone 12 represents the front row of the vials directly exposed to the freeze-dryer window. Zones 4 and 9 represent the central vials of the shelf (i.e., the vials that are less exposed to the effect of chamber walls).

In all experiments, the freezing step was carried out at a freezing rate of −1 [°C/min] down to −50 [°C]. The condenser temperature was kept at −85 [°C] during the entire freeze-drying cycle.

The following measurements were collected in each experiment:

1. Pressure: both a capacitance manometer and a Pirani gauge were used.
2. Heating fluid temperature: the silicone oil temperature was measured at the entrance of the shelf. No significant difference between this measurement and the set point of the shelf temperature was found in any of the experiments.
3. Product temperature: measurements were obtained by placing each of the 12 available thermocouple probes (T type, copper constantan wire, and AWG 24) inside 12 different vials placed in different thermal zones (Figure 1b).

Measurements were collected at a sampling interval of $\Delta t = 30$ [s]. The critical temperature for the given formulation was assumed to correspond to the formulation glass-transition temperature in the frozen state and was found to be 240.15 [K] upon characterization with differential scanning calorimetry. The maximum sublimation flow that could be processed in order to avoid choked flow conditions was obtained by performing sublimation experiments with vials filled with water on the fully loaded equipment under two different conditions of shelf temperature (kept constant during each experiment). The results are reported in Table 1.

In order to avoid the violation of this constraint, in all our simulations we used a conservative approach and assumed that

https://dx.doi.org/10.1021/acs.iecr.9b06402
Ind. Eng. Chem. Res. 2020, 59, 5056−5071

Table 1. Maximum Sublimation Flow That Can Be Processed on the Given Equipment to Avoid Choked-Flow Conditions at Different Shelf Temperatures and Chamber Pressures

shelf temperature [K]	chamber pressure [Pa]	choked-flow sublimation flow [kg/s]
233.15	6.27	1.83×10^{-5}
248.15	12.0	4.67×10^{-5}

the maximum sublimation flow is constant and equal to 1.83×10^{-5} [kg s^{-1}].

The two variables that could be manipulated in each experiment were the chamber pressure and the shelf temperature. The chamber pressure could be manipulated according to a piecewise constant profile, whereas the shelf temperature could be changed according to a piecewise linear profile. On the basis of the flexibility allowed by the equipment controller to set the recipe, a maximum of 14 switching intervals (including the initial ramp of shelf temperature after freezing) could be set for both variables.

2.2. Software. All modeling activities (model development, sensitivity analysis, parameter estimation, model validation, and dynamic optimization) were carried out using gPROMS Model Builder v. 5.1.[33] A solution for the model was obtained using the DASOLV solver,[33] which implements a backward differentiation formula. Parameter estimation was performed using a maximum likelihood estimator.[34] Dynamic optimization was carried out using a nonlinear sequential quadratic programming (NLPSQP) optimizer. All simulations were performed on an Intel Core I7-5600U CPU@2.60 GHz processor with 16.0 GB of RAM.

3. MODEL DEVELOPMENT

We identify as KPIs of primary drying the following variables:

1. Product temperature.
2. Water vapor flow triggered by sublimation.
3. Residual length of the frozen layer during sublimation.

The first two KPIs must be monitored to check for product (the former) and process (the latter) constraints, while the third KPI is an indicator of primary drying duration.

We aim at finding the simplest model (i.e., the model with the smallest number of parameters to be estimated from experimental data) that allows the relation of the process operating conditions (shelf temperature and chamber pressure) to the process KPIs under the assumptions presented in the following section.

3.1. Modeling Assumptions. The primary drying model relies on the following assumptions.

3.1.1. Assumption 1: Physical Mechanism. The only physical mechanism involved during primary drying is sublimation. Water desorption was assumed to be negligible since the desorption kinetics is very slow in the temperature range (<−5 °C) in which primary drying is carried out.

3.1.2. Assumption 2: Sublimation Interface. Sublimation occurs only at the interface between the frozen layer and the dried product, and this interface is flat along the entire vial surface.

3.1.3. Assumption 3: Impact of the Stoppering. The mass-transfer resistance imposed by the stopper is the same for all of the vials in the lot. Moreover, on the basis of the experimental findings of Pikal et al.[26] and Scutellà et al.,[35] the contribution of the stopper to the overall mass-transfer resistance is expected to be significantly smaller than the resistance imposed by the dried product.

3.1.4. Assumption 4: Heat-Transfer Mechanism. Following Pikal et al.,[36] the contributions to heat transfer due to convection are neglected. Therefore, the only heat-transfer mechanisms are conduction and radiation.

3.1.5. Assumption 5: Thermal Radiation. The chamber walls, the rails, and the shelves can be treated as black bodies, and radiation and absorption occur within the same spectral range. Under these circumstances, the Stefan−Boltzmann law holds true. Moreover, a negligible contribution to radiation occurs from the water vapor inside the drying chamber and from adjacent vials.

3.1.6. Assumption 6: Wall Temperature. The temperature of the drying chamber walls is constant. This assumption was verified experimentally by placing some thermocouples at different wall locations inside the drying chamber in some primary drying experiments. No significant difference in wall temperature (±3 °C) among different wall locations was found.

3.1.7. Assumption 7: Radial Gradients of Temperature and Ice Distribution. There are no radial gradients of temperature or of ice distribution within the product matrix.[9]

3.1.8. Assumption 8: Axial Gradients of Temperature. The product temperature is equal to the vial bottom temperature, and the temperature gradient between the bottom of the vial and the sublimation interface is negligible. This assumption holds true when the heat transfer along the frozen layer is much faster than the heat transfer between the shelf and the bottom of the vial, as in the case of many pharmaceutical formulations.[25,35]

3.1.9. Assumption 9: Water Vapor Flow from the Vial to the Condenser. The flow of water vapor from each vial to the condenser is assumed to be one-dimensional. As proven by Trelea et al.,[37] this assumption works reasonably well when the condenser is separated from the drying chamber by a pipe, as for the equipment used for this study. Moreover, as confirmed by previous studies based on computational fluid dynamics simulations,[38,39] it is assumed that the variation of total pressure between the chamber and the condenser is negligible compared to the variation of water vapor partial pressure and that there are no significant pressure leaks in the chamber.

3.1.10. Assumption 10: Ideal Gas Behavior. The water vapor and the inert gas (i.e., nitrogen) inside the drying chamber are assumed to follow the ideal gas law. This assumption is justified by the very low operating pressure.

3.1.11. Assumption 11: Shelf Temperature. The shelf temperature is assumed to be uniform over the entire shelf.

3.1.12. Assumption 12: Heat Capacity of the Glass Vial. The heat capacity of the glass vial is assumed to be constant.

3.2. Mathematical Model. In this section, we first present the model equations that describe heat and mass transfer in a single vial. Then, we describe the dynamics of the water vapor partial pressure. Finally, we provide a structural analysis of the proposed model.

3.2.1. Heat Transfer. Following assumptions 4−7, in a single vial a dynamic energy balance for the frozen layer can be derived according to the equation

$$\rho_f c_{p,f} A_v \frac{d(L_f T_p)}{dt} = \dot{Q}_s + \dot{Q}_w + \dot{Q}_r - \Delta H_{sub} J_w A_v \quad (1)$$

where ρ_f [kg m^{-3}] is the density of the frozen product, $c_{p,f}$ [J kg^{-1} K^{-1}] is the ice specific heat capacity, A_v [m^2] is the cross-sectional area of the vial, L_f [m] is the length of the frozen layer, T_p [K] is the product temperature, ΔH_{sub} [J kg^{-1}] is the heat of sublimation, and J_w [kg m^{-2} s^{-1}] is the sublimation flux. The

https://dx.doi.org/10.1021/acs.iecr.9b06402
Ind. Eng. Chem. Res. 2020, 59, 5056−5071

three terms $\dot{Q}_s$, $\dot{Q}_w$, and $\dot{Q}_r$ represent the thermal rates derived from the interaction of the vial with the upper and lower shelves, the chamber walls, and the rails, respectively. Note that, unlike other authors,[10,21,31] in eq 1 we removed the assumption of pseudo-steady-state conditions (i.e., heat flow supplied to the vial = heat flow required by sublimation), thus allowing product temperature variation during transient operating conditions.

The thermal contribution from the chamber walls is a pure radiant contribution that, according to assumption 7, can be described using a simplified expression of the Stefan−Boltzmann law

$$\dot{Q}_w = a_1\sigma_{SB}(\overline{T}_w^{\,4} - T_p^{\,4}) \tag{2}$$

where a_1 [m^2] is an equipment-dependent parameter that needs to be estimated from experimental data, σ_{SB} [$W\ m^{-2}\ K^{-4}$] is the Stefan−Boltzmann constant, and $\overline{T}_w$ [K] is the mean temperature of the chamber walls. Note that a_1 can be interpreted as the product between the emissivity of the walls and the lateral area of the vial directly exposed to radiation.

Contribution $\dot{Q}_r$ can be described in a similar fashion according to the equation

$$\dot{Q}_r = a_2\sigma_{SB}(\overline{T}_r^{\,4} - T_p^{\,4}) \tag{3}$$

where $\overline{T}_r^{\,4}$ is the mean temperature of the rails. As for a_1, a_2 [m^2] is an equipment-dependent parameter that must be estimated from experimental data.

The heat transfer between the shelf and the vial involves both conduction and radiation mechanisms. Conduction occurs at the points of contact between the shelf and the vial as well as through the gas trapped at the bottom of the vial. Recent studies[12,40] have shown that this contribution plays a key role in the overall heat transfer. Mathematically, the contribution due to conduction $\dot{Q}_{sv}$ [W] can be described according to

$$\dot{Q}_{sv} = K_v A_v(T_{shelf} - T_p) \tag{4}$$

where K_v [$W\ m^{-2}\ K^{-1}$] is the effective heat-transfer coefficient between the shelf and the vial, which can be described as a function of total chamber pressure P_c according to an experimentally validated nonlinear expression[1,21] of the form

$$K_v = C_1 + \frac{C_2 P_c}{1 + C_3 P_c} \tag{5}$$

where C_1 [$W\ m^{-2}\ K^{-1}$], C_2 [$W\ m^{-2}\ K^{-1}\ Pa^{-1}$], and C_3 [Pa^{-1}] are equipment-dependent parameters that must be calibrated from experimental data. Radiation occurs from both the top and bottom shelves. According to different authors,[10,16,31] eq 5 implicitly embeds the conduction through the vial glass and the radiant contribution from the top and bottom shelves in coefficient C_1, which is reasonable when the shelf temperature T_{shelf} is time-invariant. However, when T_{shelf} is time-varying, the radiation term needs to be modeled independently according to the Stefan−Boltzmann expression

$$\dot{Q}_{sr} = a_3\sigma_{SB}A_v(T_{shelf}^{\,4} - T_p^{\,4}) \tag{6}$$

where a_3 [−] is an equipment-dependent parameter to be estimated.

Remembering assumption 8, if we define the effective heat-transfer coefficient due to radiation from the top and bottom shelves as

$$K_r = a_3\sigma_{SB}(T_{shelf} + T_p)(T_{shelf}^{\,2} + T_p^{\,2}) \tag{7}$$

then the total heat flow rate from the shelves to the vial $\dot{Q}_s$ can then be expressed as

$$\dot{Q}_s = \dot{Q}_{sv} + \dot{Q}_{sr} = (K_v + K_r)A_v(T_{shelf} - T_p) \tag{8}$$

Note that eq 8 assumes that both mechanisms (radiation and conduction) involve the same heat-transfer area A_v.

3.2.2. Mass Transfer. As far as the sublimation front progresses, the length of the frozen layer decreases up to the point where it reaches the bottom of the vial. The time evolution of the length of the frozen layer L_f [m] can be described according to the equation proposed by Fissore et al.[21]

$$\frac{dL_f}{dt} = -\frac{1}{\rho_f - \rho_d}J_w \tag{9}$$

where ρ_d [kg/m^3] is the density of the dried product. The sublimation flux J_w can be computed according to

$$J_w = \frac{1}{R_p}(p_{w,in} - p_{w,c}) \tag{10}$$

In eq 10, $p_{w,in}$ [Pa] represents the partial pressure of the water vapor at the sublimation interface, $p_{w,c}$ [Pa] represents the partial pressure of water inside the drying chamber, and R_p [$m\ s^{-1}$] represents the resistance to mass transfer for water vapor. R_p is a function of the length of the dried layer L_d [m] according to the expression[1]

$$R_p = R_0 + \frac{R_1 L_d}{1 + R_2 L_d} \tag{11}$$

where R_0 [$m\ s^{-1}$], R_1 [s^{-1}], and R_2 [m^{-1}] are fitting parameters to be estimated from experimental data and L_d is related to L_f by the relationship

$$L_d = L_0 - L_f \tag{12}$$

where L_0 [m] is the initial length of the frozen layer, which can be easily computed from the initial volume of product inside the vial. Note that parameter R_0 represents the resistance to mass transfer of the frozen product at the beginning of sublimation (i.e., when $L_d = 0$); therefore, its value depends on the formulation considered.

The water partial pressure at the sublimation interface $p_{w,in}$ can be related to the sublimation interface temperature through the Goff−Gratch equation.[41] Following assumption 8, in this study $p_{w,in}$ was related to T_p according to the expression proposed by Velardi and Barresi:[15]

$$p_{w,in} = \exp\left(-\frac{6139.9}{T_p\ [K]} + 28.8912\right) \tag{13}$$

3.2.3. Water Vapor Partial Pressure Dynamics. Unlike other authors,[10,21,31] in eq 10 we do not assume $p_{w,c}$ to be equivalent to the total pressure inside the drying chamber. The dynamics of the water vapor partial pressure is instead modeled according to the dynamic material balance proposed by Trelea et al.[37] based on assumptions 9 and 10

$$\frac{dp_{w,c}}{dt} = \frac{R_g\overline{T}_w}{V_c M_w}(\dot{m}_s^{tot} - \dot{m}_{cd}) \tag{14}$$

where R_g [$J\ mol^{-1}\ K^{-1}$] is the ideal gas constant, V_c [m^3] is the volume of the drying chamber, M_w [$kg\ kmol^{-1}$] is the molar mass of water, $\dot{m}_s^{tot}$ [$kg\ s^{-1}$] is the total water vapor flow generated by the sublimation of all of the vials inside the drying chamber, and

https://dx.doi.org/10.1021/acs.iecr.9b06402
Ind. Eng. Chem. Res. 2020, 59, 5056−5071

$\dot{m}_{cd}$ [kg s^{-1}] is the water vapor flow that is removed at the surface of the condenser.

The total water vapor flow due to sublimation can be computed as the sum of the single contributions of each vial inside the drying chamber

$$\dot{m}_s^{tot} = \sum_{n=1}^{N_v} \dot{m}_s^{(n)} = \frac{\pi d_v^2}{4} \sum_{n=1}^{N_v} J_w^{(n)} \quad (15)$$

where N_v is the total number of vials and $\dot{m}_s^{(n)}$ and $J_w^{(n)}$ are the sublimation flow and sublimation flux of the nth vial inside the chamber, respectively.

Under assumptions 9 and 10, the condensed water vapor flow $\dot{m}_{cd}$ [kg s^{-1}] can be computed according to the expression[37]

$$\dot{m}_{cd} = \frac{1}{\alpha \bar{T}_{cd}} \log \frac{(P_c - p_{w,cd})}{(P_c - p_{w,c})} \quad (16)$$

where $p_{w,cd}$ [Pa] is the water partial pressure at the condenser interface, $\bar{T}_{cd}$ [K] is the mean temperature of the condenser, and α [Pa s kg^{-1} K^{-1}] is an equipment-dependent parameter that needs to be estimated from experimental data. Note that $p_{w,cd}$ can be related to $\bar{T}_{cd}$ using the Goff−Gratch equation or eq 13.

Also note that eq 16 is structurally similar to the one proposed by Trelea et al.[37] However, different from what these authors reported, parameter α in eq 16 does not embed the total chamber pressure P_c since we assume that P_c may be time-varying.

3.2.4. Model Structure. To summarize, the proposed primary drying model is composed by the set of eqs 1−16. Structurally, the model is a differential algebraic system of equations that involves two input variables (T_s and P_c), three KPIs (T_p, $\dot{m}_{sub}^{tot}$, and L_f), and nine model parameters to be estimated from experimental data (R_1, R_2, α, C_1, C_2, C_3, a_1, a_2, and a_3). All other model parameters (physical constants, formulation-dependent parameters, and equipment-dependent parameters) are fixed, and their values are reported in Table 2. Note that since we considered the same formulation in all experiments, parameter R_0 can be considered to be fixed, and its value was obtained from the literature.[42]

4. SENSITIVITY ANALYSIS

Sensitivity analysis can be used to understand how the variability of the process KPIs can be allocated to the different model parameters.[43] Once the parameters that are most influential toward the KPIs are identified, we can focus on strengthening the accuracy of their estimation. On the other side, parameters that have little or no effect on the KPIs can be discarded from the parameter estimation activity and fixed to their nominal values without significantly compromising the prediction fidelity of the model.

Sensitivity analysis techniques can be categorized into two different groups: local and global. Local sensitivity analysis considers one parameter at a time and consists of imposing a small perturbation on the selected parameter around its nominal value and quantifying its effect on the selected KPI in terms of partial derivatives. Global methodologies consist of varying all of the model parameters simultaneously over the entire parameter domain and quantifying both the effect of single parameters and the effect of their interactions with respect to the selected KPI.

In this study, we perform a GSA over the entire parameter space. We use Sobol's method.[44] According to this methodology, the variance $V(y_j)$ of the jth KPI (j = 1,..., N_J where N_J is the total number of selected KPIs) is decomposed according to the expression

$$V(y_j) = \sum_{k=1}^{K} V_k + \sum_{1 \le l \le m \le K}^{K} (V_{l,m} + ... + V_{l,m,...,K}) \quad (17)$$

where V_k, with k = 1,..., K, is the contribution to the variance of the jth KPI solely related to the kth model parameter and $V_{l,m}$ is the contribution to the output variance due to interaction between the lth and mth parameters. The results of Sobol's GSA are collected by two different metrics: first-order sensitivity index S_k, which accounts for the direct effect of the kth parameter on the KPI, and total sensitivity index $S_{T,k}$, which accounts for the direct effect of the kth parameter on the KPI as well as the effect due to the interaction of the kth parameter with the other model parameters. Both metrics are computed using Monte Carlo simulations based on initial user-defined distributions. The number of model evaluations for each iteration is $N_s(K+2)$, where N_s is a user-defined number of samples for each parameter distribution and K is the number of parameters. Details on the mathematical derivation of these two metrics can be found in Sobol[45] and Saltelli et al.[46]

From a practical perspective, the greater $S_{T,k}$, the greater the influence of the kth parameter on the selected KPI. The values of $S_{T,k}$ fall within the range of [0, 1]. When dynamic models are considered, as occurs in this study, the values of $S_{T,k}$ can be computed at different time intervals over an assigned time horizon.

Table 2. List of Fixed Model Parameters and Their Respective Values

parameter	symbol	value	units
Physical Constants			
ideal gas law constant	R_g	8.3145	[J mol^{-1} K^{-1}]
Stefan−Boltzmann constant	σ_{SB}	5.6704 × 10^{-8}	[W m^{-2} K^{-4}]
molecular weight of water	M_w	18.01	[kg kmol^{-1}]
Formulation-Dependent Physical Properties			
density of the dried product	ρ_d	917	[kg m^{-3}]
density of the frozen product	ρ_f	63	[kg m^{-3}]
conductivity of the frozen product	λ_f	2.47	[W m^{-1} K^{-1}]
heat of sublimation	ΔH_s	2.838 × 10^6	[J kg^{-1}]
specific heat capacity of the frozen product	$c_{p,f}$	2108	[J kg^{-1} K^{-1}]
mass-transfer resistance of the frozen product	R_0	5.12 × 10^4	[m s^{-1}]
Equipment-Dependent Fixed Parameters			
vial diameter	d_v	0.01455	[m]
chamber volume	V_c	0.118	[m^3]
mean wall temperature	$\bar{T}_w$	276.15	[K]
mean rail temperature	$\bar{T}_r$	250.15	[K]
mean condenser temperature	$\bar{T}_{cd}$	188.15	[K]

4.1. Results of Sensitivity Analysis for the Primary Drying Model. Dynamic Sobol's GSA was implemented for the nine model parameters (R_1, R_2, α, C_1, C_2, C_3, a_1, a_2, and a_3) with respect to the three KPIs (T_p, $\dot{m}_s^{tot}$, L_f). Note that $\dot{m}_s^{tot}$ was simply computed as the product of the sublimation flow of a single vial and the number of vials. Uniform distributions for the model parameters were assumed, and the bounds of these distributions can be found in Table 3. These bounds were chosen on the basis of typical values of the model parameters that can be found in published studies.[36,40] It is worth noticing that the choice of these ranges directly affects the values of the sensitivity indices

https://dx.doi.org/10.1021/acs.iecr.9b06402
Ind. Eng. Chem. Res. 2020, 59, 5056−5071

Table 3. Bounds for the Uniform Distributions of the Model Parameters Used for Sobol's Global Sensitivity Analysis

parameter	bounds	units
R_1	$[1 \times 10^8, 9\times 10^8]$	$[s^{-1}]$
R_2	$[1 \times 10^2, 1 \times 10^4]$	$[m^{-1}]$
α	[1000, 3000]	$[s\ kg^{-1}\ K^{-1}]$
C_1	[0, 10]	$[W\ m^{-2}\ K^{-1}]$
C_2	[0, 2]	$[W\ m^{-2}\ K^{-1}\ Pa^{-1}]$
C_3	[0, 2]	$[Pa^{-1}]$
a_1	$[1\times 10^{-5}, 9 \times 10^{-5}]$	$[m^2]$
a_2	$[1\times 10^{-5}, 9\times 10^{-5}]$	$[m^2]$
a_3	$[1\times 10^{-5}, 9 \times 10^{-5}]$	[−]

obtained with the GSA[47] but not the qualitative considerations that can be drawn from them.

Fixed values of shelf temperature (250.15 [K]) and chamber pressure (10 [Pa]) were assigned to perform the analysis. The analysis was implemented using 100 × (9 + 2) = 1100 samples. Dynamic sensitivities were collected every 10 [min] over a time horizon of 500 [min]. Due to the limited computational time required for a single model evaluation, the GSA took less than 10 [h] to complete.

We report the time profiles of the total sensitivity indices $S_{T,k}$ for all parameters with respect to each KPI.

Figure 2a shows the dynamic profiles of the total sensitivity indices for the product temperature. As expected, the radiation from the chamber walls (parameter a_1), the radiation from the upper and lower shelves (parameter a_3), and the conduction through the gas trapped at the bottom of the vial (parameter C_2) affect the product temperature, with parameter a_1 being the most influential. Product temperature is also strongly affected by mass-transfer parameter R_1. This can be easily understood by considering that for high values of R_1 sublimation is inhibited; therefore, a large portion of the total heat flux supplied to the vial is used to increase the product temperature, as described by eq 1. On the other side, parameter R_1 has little or no effect on the product temperature, as well as parameters C_3, a_2, and α.

The sensitivity plot for the sublimation flow (Figure 2b) shows that parameters a_1, α, R_1, and C_2 affect this KPI, with a_1 again being the most influential. When a_1 increases, the following quantities increase as well: heat flux to the product, product temperature (for the same sublimation energy requirement), partial pressure at the sublimation interface (according to eq 13), driving force for sublimation, and sublimation flow. Note that parameter α, which hardly affects the product temperature, strongly impacts the sublimation flow.

Figure 2c shows the sensitivity plot for the last KPI (i.e., the length of the frozen layer). The results show that mass-transfer parameter R_1 has a strong influence on this KPI, as well as parameters a_1, C_2, and α. Considerations similar to those for the sublimation flow can be used. Note that, different from the other KPIs, parameter C_1 has a minor impact on the length of the frozen layer.

A thorough analysis of the results of the GSA allows us to draw the following general conclusions for the primary drying model (eqs 1−16):

1. The parameters showing the greatest sensitivity toward the three KPIs are thermal radiation parameter a_1 and mass-transfer parameter R_1, with a_1 being the most influential.
2. Heat-transfer parameters C_3 and a_2 have a negligible effect on the KPIs. Therefore, their values have little effect on the model predictions.
3. Mass-transfer parameter R_2 has a negligible effect on the KPIs. Note that this is in agreement with the experimental findings of Scutellà et al.[35]
4. Each of the remaining parameters (C_1, C_2, a_3, and α) significantly affects at least one KPI; therefore, their values must be estimated with good accuracy to guarantee good model prediction fidelity.

5. EFFECT OF DRYING HETEROGENEITY

The deployment of eqs 1−16 for process simulation and optimization requires knowing the contribution of each vial to the total sublimation flow expressed by eq 15. In principle, if all the vials inside the drying chamber had the same behavior, then the total sublimation flow could be computed as the product of the sublimation flow from a single vial and the total number of vials. However, vials placed at different locations of the shelf exhibit different sublimation rates; therefore, the computation of the total sublimation flow (eq 15) needs to account for this intralot drying heterogeneity.

Vials located on the border of the shelves receive radiant heat from the chamber walls and from the rails, as well as additional

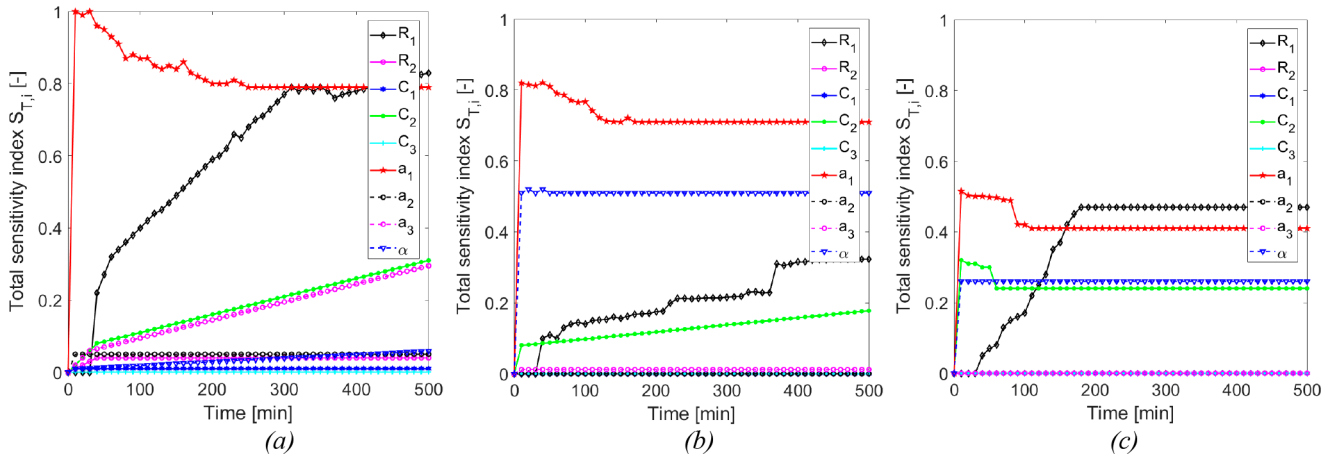

Figure 2. Sobol's total sensitivity indices for the nine parameters of the primary drying model with respect to (a) product temperature, (b) total sublimation flow, and (c) length of the frozen layer.

https://dx.doi.org/10.1021/acs.iecr.9b06402
Ind. Eng. Chem. Res. 2020, 59, 5056−5071

heat due to conduction through the water vapor between the rails and the side wall of the vials.[26] On the other side, vials placed in the center of the shelves are shielded by the adjacent vials; therefore, they do not receive these additional heat flow contributions. From a modeling perspective, these different heat-transfer mechanisms result in different values of the heat-transfer parameters between edge and central vials.[16] Moreover, as experimentally verified by several authors,[1,25,35] the value of the mass-transfer resistance (eq 11) can vary significantly among vials placed at different locations.

Accounting for drying heterogeneity in the modeling framework would require identifying each physical mechanism responsible for intralot variability and allocating this variability to the specific parameter or equation of the model representing that physical mechanism. An attempt in this direction has been recently proposed by Scutellà et al.[48] However, detailed knowledge of all sources of intralot variability requires extensive experimentation and incurs the risk of obtaining uncertainty distributions for the model parameters that compromise their statistical meaning.[48] In this study, we use a simplified yet effective approach to address this problem.

For the purpose of primary drying optimization, the main target is to guarantee that the time profiles of the KPIs are correctly predicted by the model, independently of how the uncertainty (due to intralot variability) is allocated within the model formulation. This target can be obtained by allocating uncertainty to the parameter with the greatest sensitivity toward the KPIs. The higher the influence of the parameter on the KPIs, the narrower the uncertainty distribution that is needed to describe intralot variability without compromising the prediction fidelity of the model.

The GSA results showed that the most influential parameter is a_1 (i.e., the parameter describing the effect of radiation from the chamber walls). Therefore, we introduce a stochastic description of this parameter without making any further modification to the model structure. We assume a normal distribution of a_1 with mean $\overline{a}_1$ and standard deviation σ_{a_1} (i.e., $a_1 \approx N(\overline{a}_1, \sigma_{a_1})$. Both $\overline{a}_1$ and σ_{a_1} are treated as parameters to be estimated from experimental data. Monte Carlo simulations are used to sample as many stochastic scenarios as the number of vials inside the drying chamber (namely, 476). Each stochastic scenario requires solving eqs 1−13 in order to predict at each time point the single-vial sublimation flux described by eq 10; once each scenario is solved, the total sublimation flow can be computed according to eq 15. A schematic representation of the proposed multivial stochastic approach is shown in Figure 3.

Note that, using this approach, we cannot relate each stochastic scenario directly to the actual position of the vial inside the drying chamber.

6. MODEL CALIBRATION

On the basis of the results of the GSA, parameters R_2, C_3, and a_2 could be discarded from the parameter estimation activity. The remaining seven parameters were collected in parameter vector $\boldsymbol{\theta} = (C_1, C_2, \overline{a}_1, \sigma_{a_1}, a_3, R_1, \text{and } \alpha)$ and considered for estimation.

Two experiments with piecewise time-varying profiles of the manipulated inputs were used to calibrate the model. The experiments were not specifically designed for stochastic model calibration, but they were simply meant to capture the main dynamics of the drying process. Their recipes (in terms of time profiles of shelf temperature and chamber pressure) are shown in Figures 4a and 5a.

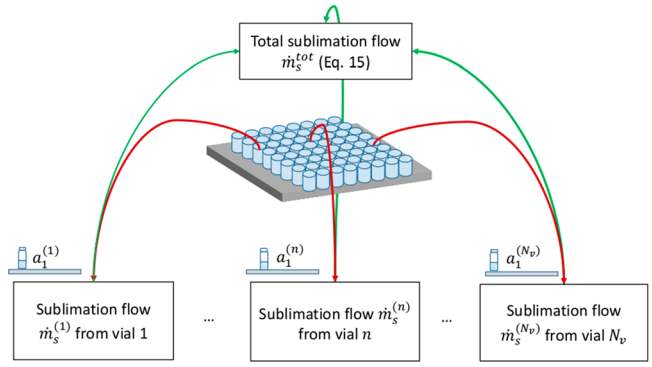

Figure 3. Schematic representation of the multivial stochastic model used to describe drying heterogeneity.

Primary drying started at a shelf temperature of 223.15 [K] in both experiments. We used only two measurements to estimate the model parameters:

1. Water partial pressure inside the drying chamber;
2. Product temperature collected for the zone exposed to the window (zone 12; i.e., maximum product temperature).

Measurements of water partial pressure were inferred from the readings of the Pirani gauge and capacitance manometer following the binary gas transport model proposed by Trelea et al.[37] According to this model, if the Pirani gauge is calibrated at low pressure with pure nitrogen (as for our equipment), then the relationship between the water vapor partial pressure and the Pirani and capacitance readings can be expressed as

$$p_{w,c}^{exp} = \frac{(p^{Pirani} - p^{CM})}{\left(\frac{\lambda_w^v}{\lambda_{N_2}} - 1\right)} \tag{18}$$

where $p_{w,c}^{exp}$ is the experimental value of the water vapor partial pressure, p^{Pirani} is the Pirani reading, p^{CM} is the reading of the capacitance manometer, λ_w^v [W m^{-1} K^{-1}] is the thermal conductivity of water vapor, and λ_{N_2} is the thermal conductivity of nitrogen. Ratio $\frac{\lambda_w^v}{\lambda_{N_2}}$ is equal to 1.6; therefore, eq 18 simplifies to

$$p_{w,c}^{exp} = \frac{(p^{Pirani} - p^{CM})}{0.6} \tag{19}$$

Measurements were filtered with a moving-average low-pass filter with a window size equal to 10 min. Model predictions of water partial pressure as expressed by eq 14 were challenged with respect to these measurements.

The product temperature measurements for zone 12 were fitted with the model-based trajectory of the stochastic scenario with the highest product temperature at any time during sublimation. The underlying assumption that we made is that the vial exposed to the window where the thermocouple is placed can be considered to be the vial where the highest product temperature is experienced within the lot. This allowed us to obtain a good indicator of where the product temperature constraint could be first violated.

The estimated values of the model parameters, together with their 95% confidence intervals and t values, are reported in Table 4.

It can be observed that the t values of all of parameters are greater than the reference t value, meaning that the precision in their estimation is statistically satisfactory. This is also confirmed by the narrow confidence intervals obtained for all parameters.

https://dx.doi.org/10.1021/acs.iecr.9b06402
Ind. Eng. Chem. Res. 2020, 59, 5056−5071

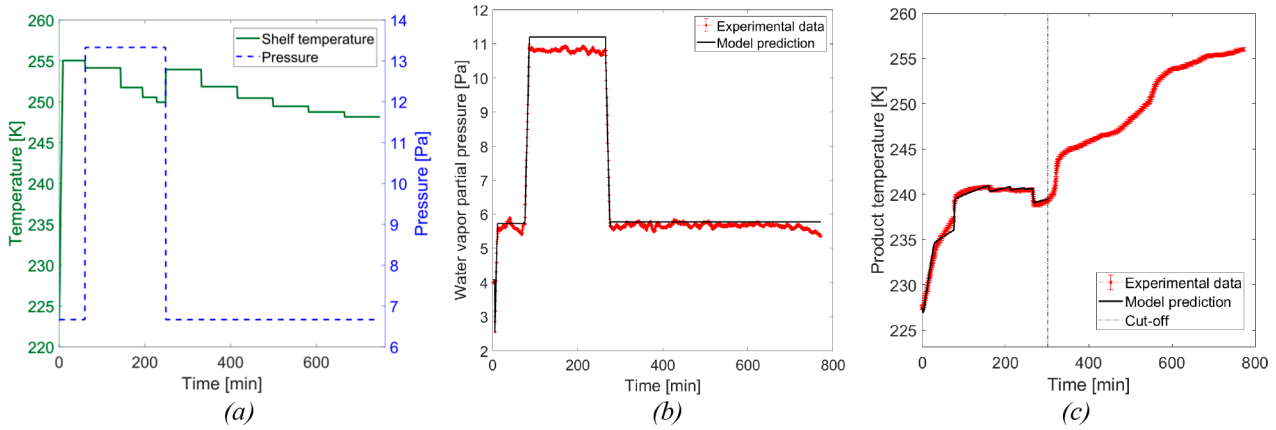

Figure 4. First calibration run. (a) Recipe for the experiment. (b) Comparison of the predicted profile of water vapor partial pressure and the experimental observations. (c) Comparison of the predicted profile of the maximum product temperature and the experimental observations.

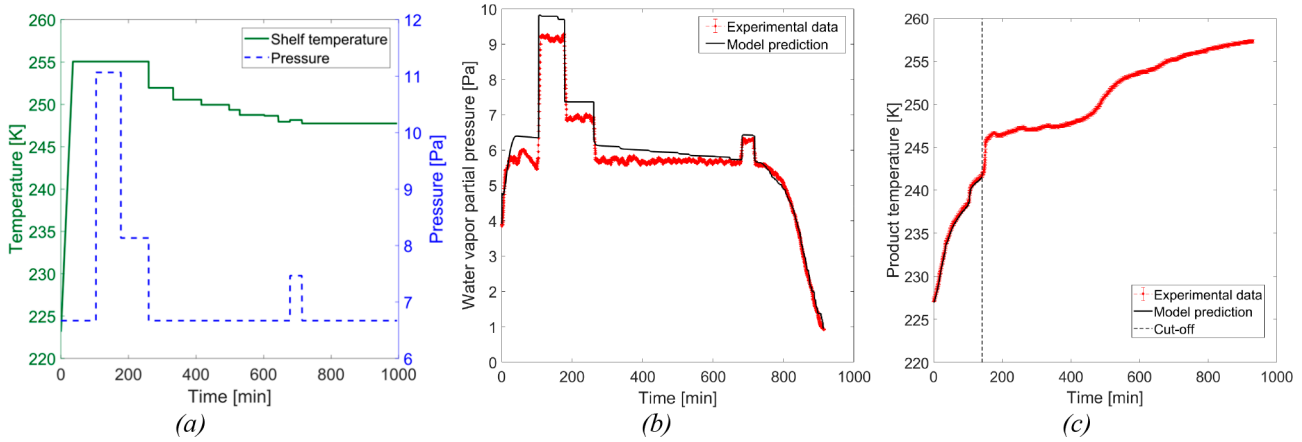

Figure 5. Second calibration run. (a) Recipe for the experiment. (b) Comparison of the predicted profile of water vapor partial pressure and the experimental observations. (c) Comparison of the predicted profile of the maximum product temperature and the experimental observations.

Table 4. Estimated Values of the Model Parameters with Their 95% Confidence Intervals (CIs) and *t* Values

parameter	units	value	95% CI	*t* value
C_1	[W m^{-2} K^{-1}]	2.825	±0.112	39.70
C_2	[W m^{-2} K^{-1} Pa^{-1}]	0.215	±0.09	31.20
$\overline{a}_1$	[m^2]	7.625×10^{-5}	$\pm 8.213 \times 10^{-7}$	25.12
σ_{a_1}	[m^2]	1.545×10^{-5}	$\pm 9.416 \times 10^{-7}$	12.36
a_3	[−]	2.723×10^{-6}	$\pm 1.014 \times 10^{-7}$	4.12
R_1	[s^{-1}]	3.288×10^{8}	$\pm 8.935 \times 10^{6}$	68.12
α	[Pa s kg^{-1} K^{-1}]	2580	±15	11.30
			reference *t* value (95%)	1.645

The comparison between the model predictions of water vapor partial pressure and maximum product temperature and the experimental data for the first test run are shown in Figure 4.

Both the water vapor partial pressure (Figure 4b) and the maximum product temperature (Figure 4c) were predicted with good accuracy. Note that we used only the temperature observations that were measured before the sublimation front crossed the tip of the thermocouple for model calibration. The crossing of the thermocouple by the sublimation front is identified by the point of inflection of the temperature trajectories ("cut-off" in Figure 4c). From this point on, the temperature measurements no longer refer to the frozen product; therefore, the measured temperature profile cannot be captured with the model.

Good agreement between the model trajectories and the experimental observations was also obtained for the second test run (Figure 5b,c). In particular, the decrease in the water partial pressure at the end of primary drying (starting after ∼700 [min]) was correctly predicted by the model, suggesting that the stochastic distribution of the residual ice content for the 476 vials was captured with good accuracy.

Figure 6 shows the correlation matrix of the model parameters.

The analysis of this matrix suggests some considerations. First, it can be observed that the heat-transfer parameters (particularly C_2, $\overline{a}_1$, σ_{a_1}, and a_3) are significantly correlated with mass-transfer parameter R_1. Evidence of the correlation between heat- and mass-transfer parameters questions the common industrial

https://dx.doi.org/10.1021/acs.iecr.9b06402
Ind. Eng. Chem. Res. 2020, 59, 5056−5071

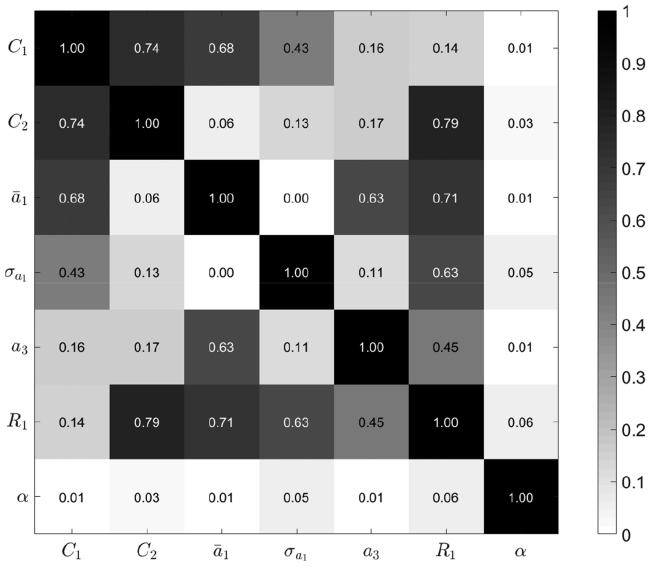

Figure 6. Correlation matrix of the model parameters estimated with the two historical test runs.

practice of inferring the values of the mass-transfer parameters from the gravimetric values of the heat-transfer parameters. Stated differently, uncertainty in the gravimetric values of the heat-transfer parameters will considerably impact the accuracy of the values of the mass-transfer parameters inferred from temperature data. This problem has recently been discussed by Trelea et al.[37]

Second, the strong correlation between the two parameters with the greatest sensitivities toward the KPIs (namely, a_1 and R_1) supports the choice of describing intralot variability as parametric uncertainty in a_1 only. In fact, the stronger the correlation between these two parameters, the greater the flexibility in allocating to parameter a_1 the sources of variability that would impact mass-transfer parameter R_1 (e.g., due to different cake resistances in different vials).

Third, it can be observed that parameter α is almost independent of the other model parameters. This suggests that its value can be estimated with high accuracy separately from the other model parameters. This is in line with the recent experimental findings of Trelea et al.[37] Finally, it should be noticed that the parameters with the strongest correlation are C_2 and R_1 (i.e., the parameters describing the dependence of the heat- and mass-transfer mechanisms on the operating conditions).

7. MODEL VALIDATION

The prediction fidelity of the calibrated model was assessed using historical primary drying experiments that were not used for calibration purposes. The recipe for one of these experiments is shown in Figure 7a. Figure 7b,c shows the comparison between the model-predicted trajectories and the experimental observations of water partial pressure and maximum product temperature, respectively.

Both trajectories were captured with good accuracy, even though the maximum product temperature was slightly overestimated before the cutoff, thus suggesting a potential lower prediction fidelity of the model toward this KPI.

To assess the model robustness, the validation was repeated in two other primary drying experiments. Overall, the consistency of performance with different historical test runs confirmed the reliability of the model.

7.1. Model Reusability. Within an industrial environment, the reusability of the proposed mathematical model with different product formulations and/or pieces of equipment requires (i) historical test runs obtained with dynamic perturbations of the manipulated inputs and (ii) a maximum likelihood estimator.

Different test runs implemented with different product formulations and/or pieces of equipment showed that, in most situations, a single test run can be sufficient to obtain a satisfactory estimation of the entire parameter vector $\boldsymbol{\theta} = (R_1, C_1, C_2, \bar{a}_1, \sigma_{a_1}, a_3, \alpha)$. Note that, due to the high correlation between heat- and mass-transfer parameters, a re-estimation of all parameters in $\boldsymbol{\theta}$ is required whenever a change in product formulation or equipment is considered. It is worth noticing that the number of parameters that need recalibration with the proposed modeling framework is comparable to that required with the monodimensional models available in the literature (typically, these models require estimating six parameters: three for heat transfer and three for mass transfer). However, the experimental burden required for parameter estimation with the proposed framework is significantly smaller (potentially a single primary drying experiment compared to (at least) three

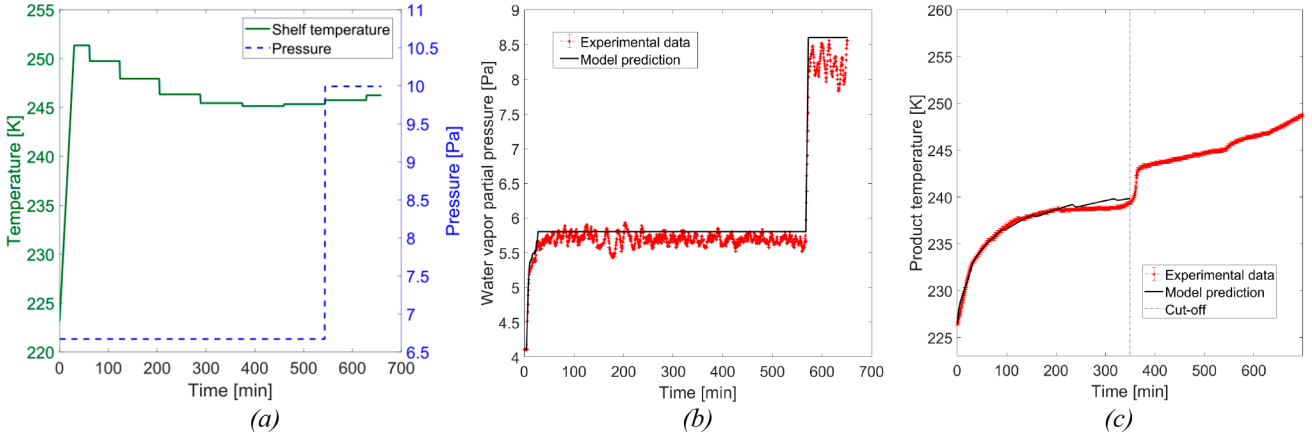

Figure 7. Model validation. (a) Recipe for the experiment. (b) Comparison of the predicted profile of water vapor partial pressure and the experimental observations. (c) Comparison of the predicted profile of the maximum product temperature and the experimental observations.

https://dx.doi.org/10.1021/acs.iecr.9b06402
Ind. Eng. Chem. Res. 2020, 59, 5056−5071

gravimetric experiments and (at least) one primary drying experiment).

8. PRIMARY DRYING OPTIMIZATION

The validated stochastic model was used to propose an optimized drying recipe to minimize process duration.

8.1. Problem Formulation. The optimization problem can be formulated as follows: find the optimal dynamic profiles of shelf temperature $T_{shelf}(t)$ and chamber pressure $P_c(t)$ that minimize the primary drying duration τ_{dry} [s] while guaranteeing that, at any time, (a) the maximum product temperature is lower than the product collapse temperature and (b) the total sublimation flow does not exceed the choked-flow value. Constraint (a) guarantees that product quality will not be compromised for any vial in the batch, whereas constraint (b) allows loss of pressure control in the drying chamber to be avoided.

The end point of primary drying was set as the time that is needed to completely remove the ice from the vial where sublimation ends last. Mathematically, this is the same as constraining the length of the frozen layer with the greatest value in all scenarios to be equal to zero at the end of primary drying.

The mathematical formulation of the optimization problem can then be described as follows

$$\min_{T_{shelf}(t),P_c(t)} \tau_{dry} \tag{20}$$

subject to:

$$\max(L_f(\tau_{dry})) = 0 \text{ [m]} \tag{21}$$

$$\max(T_p(t)) < 240.15 \text{ [K]} \tag{22}$$

$$\dot{m}_s^{tot}(t) < 1.83 \times 10^{-5} \text{ [kg s}^{-1}\text{]} \tag{23}$$

where eq 21 is an end-point equality constraint and eqs 22 and 23 are interior-point inequality constraints. To speed up convergence, the equality end-point constraint (eq 21) was converted to an inequality end-point constraint

$$\max(L_f(\tau_{dry})) < 10^{-4} \text{ [m]} \tag{24}$$

meaning that sublimation was assumed to be completed when the residual thickness of ice in the vial where the slowest sublimation occurs was smaller than 0.1 [mm].

Consistent with the equipment specifications, the trajectories of shelf temperature and chamber pressure were set to be piecewise linear and piecewise constant, respectively. Fourteen switching intervals were set for these two variables. The chamber pressure was assumed to vary in the range of 5−15 [Pa], whereas shelf temperature was assumed to vary within the range of 223.15−255.15 [K]. Primary drying was assumed to start at a shelf temperature of 223.15 [K]. Due to operational constraints on the temperature control loop, the temperature increases during the first step (initial ramp) were constrained not to exceed a heating rate of 1 [K min^{-1}]. The value of shelf temperature at the end of the initial ramp was optimized like all other steps in the drying recipe.

8.2. Optimization Results. A solution of the optimization problem (eqs 20−23) requires the evaluation of 476 stochastic scenarios for each iteration. Results were obtained after 89 iterations, corresponding to a computational time of 4.5 [h]. Convergence was slow due to the very tight constraints imposed on both product temperature (eq 22) and sublimation flow (eq 23). The optimized trajectories of shelf temperature and chamber pressure that were obtained are shown in Figure 8. Note that the 14 switching intervals in the original optimized

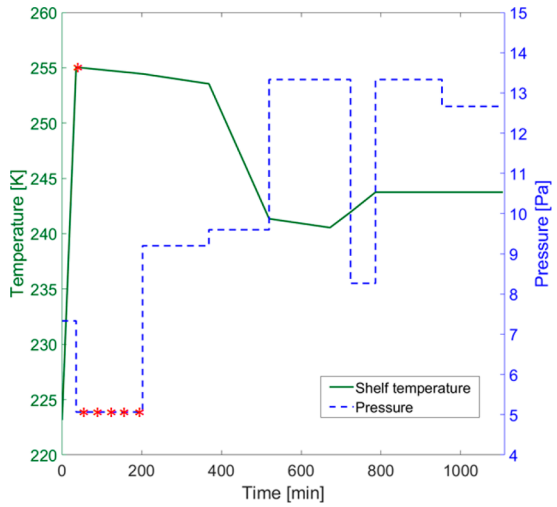

Figure 8. Trajectories of the operating conditions (shelf temperature and chamber pressure) for the time-varying optimized recipe. The red markers indicate pressure or temperature values that hit the upper or lower bounds.

recipe could be merged into only 8 switching intervals since no significant variation of the operating conditions was detected between consecutive steps suggested by the optimizer. The theoretical duration of primary drying achievable with this optimized recipe was 1106 [min], corresponding to 18.4 [h].

Figure 9 collects the corresponding model-based trajectories of the sublimation flow, water vapor partial pressure, product temperature, and length of the frozen layer for the 476 vials inside the chamber.

An inspection of the optimized recipe shows that, at first, the shelf temperature is ramped up to 255.15 [K] at constant pressure (7.33 [Pa]). After this initial step, the chamber pressure drops to its lower bound while the shelf temperature is slowly ramped down. This combination of operating conditions clearly promotes greater sublimation rates. On the other hand, Figure 9a shows that, during this initial phase, the sublimation flow is pushed very close to the choked-flow constraint, although the limiting value is never crossed. In other terms, as expected, the optimizer is pushing the sublimation rate close to the operational limits of the equipment in order to speed up the process.

In the following steps, the chamber pressure is gradually increased while the shelf temperature is gradually decreased to avoid violating the constraint on the maximum product temperature. After around 730 [min] (sixth switching interval), the chamber pressure is strongly reduced for a short period and then rapidly brought back to the value of the previous step. This behavior is necessary to avoid violating the product temperature constraint (Figure 9c). Figure 9a,b,d shows that the sublimation end point as described by the inequality constraint (eq 24) corresponds to the condition $\dot{m}_s^{tot} = 0$ but not to the condition $p_{w,c} = 0$. In fact, when $\dot{m}_s^{tot} = 0$, the decrease in the water vapor partial pressure in the chamber is delayed by the condenser dynamics (i.e., $\dot{m}_{cd} \neq 0$) as described by eqs 14 and 16. In particular, the trajectory of Figure 9b suggests that the end-point condition (eq 24) (at time t = 1106 [min]) corresponds to a decrease in the water partial pressure to about half of the steady-

https://dx.doi.org/10.1021/acs.iecr.9b06402
Ind. Eng. Chem. Res. 2020, 59, 5056−5071

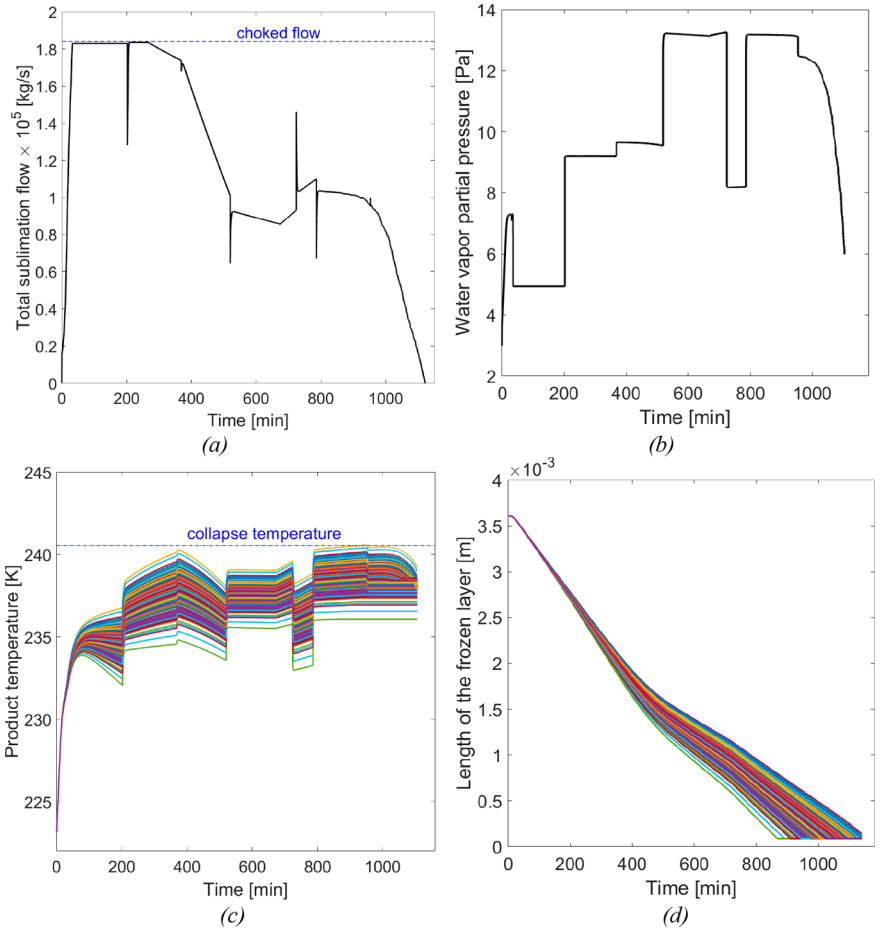

Figure 9. Model predictions of (a) total sublimation flow, (b) water vapor partial pressure, (c) product temperature for the 476 vials, and (d) length of the frozen layer for the 476 vials inside the drying chamber. The dashed lines in (a) and (c) represent the equipment and product constraints.

state value of the last switching interval (i.e., ∼12.5 [Pa]). Note that Figure 9d suggests a significant difference in the drying time required for the vial in which the fastest sublimation occurs (∼840 [min]) and the vial in which the slowest sublimation occurs (= 1106 [min]), therefore supporting the need for a description of intralot drying heterogeneity within the modeling framework.

To better understand the improvement that can be obtained with time-varying profiles of the manipulated variables with respect to the current industrial standard (i.e., time-invariant conditions), we solved the same optimization problem by enforcing time-invariant profiles for the chamber pressure and the shelf temperature (excluding the initial ramp after freezing). The resulting optimal recipe is shown in Figure 10 and suggests that the optimal time-invariant values predicted by the model are T_{shelf} = 251.15 [K] and P_c = 6.25 [Pa]. The optimal duration of primary drying with this time-invariant optimized recipe is 1332 [min] or 22.2 [h]. This result suggests that, even with an optimized recipe, the use of time-invariant operating conditions could theoretically cause an extension of the primary drying duration of ∼4 [h] (i.e., 16% increase) with respect to an optimized time-varying protocol.

8.3. Experimental Validation. *8.3.1. Base Case.* The standard (i.e., nonoptimized and routinely implemented in past experiments) operating protocol for primary drying runs used with the same formulation and the same equipment was at constant operating conditions P_c = 10 [Pa] and T_{shelf} = 255.15 [K]. Historical primary drying experiments obtained with this

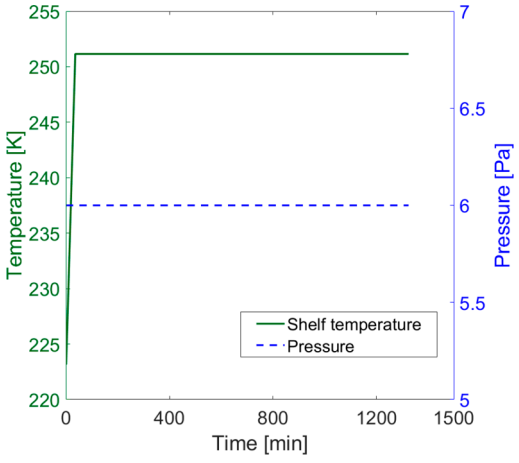

Figure 10. Trajectories of the operating conditions (shelf temperature and chamber pressure) for the time-invariant optimized recipe.

protocol showed a total duration of primary drying of ∼23 [h], thus slightly longer than the theoretical duration achievable with the time-invariant optimized recipe of Figure 10 but considerably longer than the duration achievable with the time-varying optimized recipe of Figure 8. The expected theoretical decrease in the primary drying duration with the optimized time-varying protocol with respect to this standard operating protocol was therefore 4.6 [h] or 20%.

https://dx.doi.org/10.1021/acs.iecr.9b06402
Ind. Eng. Chem. Res. 2020, 59, 5056−5071

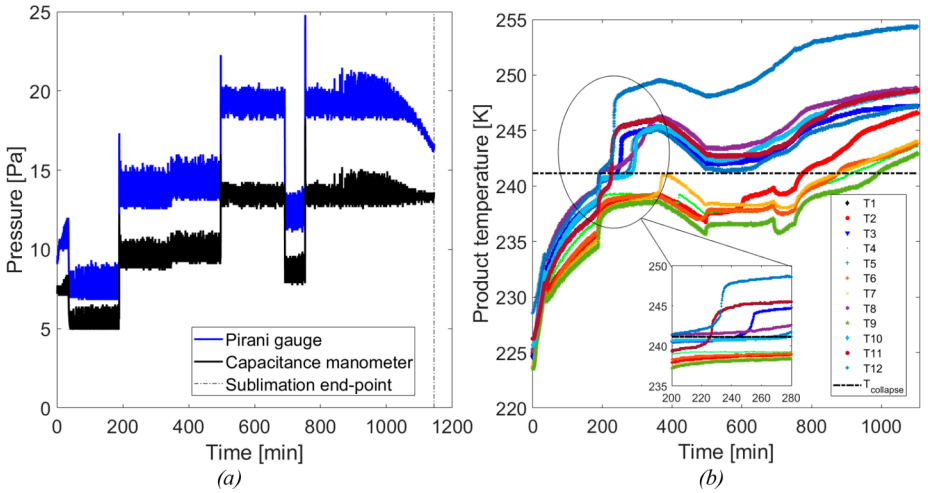

Figure 11. Optimized primary drying protocol. Experimental profiles of (a) Pirani and capacitance manometer readings and (b) product temperature for all of the thermal zones of the shelf.

Figure 12. Cake appearance for (a) the central vials and (b) the edge vials at the end of the optimized freeze-drying cycle.

8.3.2. Optimized Time-Varying Protocol. To validate the optimized time-varying protocol, we performed an experiment on the real equipment following the optimized primary drying recipe of Figure 8. Freezing was carried out at T_{shelf} = 223.15 [K]. Figure 11a shows the experimental trajectories of the readings of the Pirani and capacitance manometers, whereas Figure 11b shows the experimental profiles of product temperature for all of the thermal zones of the shelf.

The dashed line in Figure 11a represents the theoretical duration of primary drying as proposed by the optimized recipe (i.e., 1106 [min]), whereas the dashed line in Figure 11b represents the collapse temperature of the given formulation (240.15 [K]). Figure 11a shows that the sublimation end point is entirely consistent with its model-based prediction (Figure 9b), since it corresponds to a decrease of 50% of the Pirani reading. The readings of the capacitance manometer (black line) shown in Figure 11a also confirm that pressure control could be maintained for the entire drying time, meaning that the constraint on choked flow was never violated, as theoretically expected. Figure 11b shows that, for both the central (zones 4, 6, 7, and 9) and the edge vials (zones 1−3, 5, 8, 11, and 12), the constraint on the maximum product temperature was not violated. The close-up part on the same plot shows that the crossing of the sublimation front through the tip of the thermocouple for the edge vials was very close to the collapse temperature; in particular, the temperature profile for zone 12 (i.e., the zone exposed to the window) slightly crossed (∼1 [°C]) the collapse temperature. Two explanations can be given to justify this behavior. The first one is that the prediction fidelity of the model toward this KPI was not as good as theoretically expected. The second one is related to the position of the temperature probe, which most probably was not properly placed inside the vial (possibly not touching its bottom). Overall, we obtained experimental evidence of the feasibility of the proposed optimized protocol, with a significant decrease in primary drying duration with respect to the current standard.

After the optimized primary drying stage, in order to visually inspect the quality of the final product we carried out a "standard" (i.e., nonoptimized) secondary drying (T_{shelf} = 303.15 [K], P_c = 10 [Pa]), which was completed in less than 7 [h]. The visual appearance of the product for a few samples of the central (zone 9) and edge (zone 12) vials is shown in Figure 12a,b, respectively.

The visual appearance of the final product for the central vials (which are the majority of the lot) was very satisfactory. For the edge vials, a small shrinkage of the product close to the vial walls was observed (thus confirming the possibility of a slight violation of the constraint on the product temperature). However, the visual appearance of these vials was still satisfactory and comparable to that obtained with standard protocols. No single vial would have been rejected with the proposed optimized protocol.

9. CONCLUSIONS

In this study, a multivial stochastic modeling framework for the optimization of the primary drying stage of a freeze-drying process was proposed. The framework was divided into five sequential steps: model development, sensitivity analysis, model calibration, model validation, and dynamic optimization.

https://dx.doi.org/10.1021/acs.iecr.9b06402
Ind. Eng. Chem. Res. 2020, 59, 5056−5071

The novelties introduced with respect to the existing literature were the following:

1. A new semiempirical energy balance for the single vial that allows time-varying operating conditions (chamber pressure and shelf temperature) to be handled while keeping the number of equipment-dependent parameters to be estimated relatively small.
2. A modified description of the dynamic profile of the water vapor partial pressure in the chamber, stemming from the binary mixture model proposed by Trelea et al.[37]
3. A rigorous global sensitivity analysis to determine the model parameters that have the highest impact on the process KPIs (product temperature, total sublimation flux, and length of the frozen layer).
4. A stochastic approach to account for drying heterogeneity based on the allocation of intralot variability in the model formulation in terms of parametric uncertainty in the parameter with the highest sensitivity on the process KPIs.
5. A joint estimation of both heat- and mass-transfer parameters based exclusively on pressure and maximum product temperature data from single or multiple primary drying experiments.
6. A rigorous offline dynamic optimization of the drying recipe assuming time-varying operating conditions.

The proposed stochastic model was calibrated and subsequently validated with experimental data, showing good prediction fidelity. An optimal drying recipe was obtained with the proposed model and implemented experimentally. Results showed a reduction of the total drying duration with the proposed recipe of ∼20% with respect to standard drying protocols (i.e., time-invariant operating conditions) while avoiding constraint violations on both the maximum product temperature and choked flow conditions. The reusability of the proposed modeling framework with different pieces of equipment and/or different formulations requires the estimation of only seven model parameters from potentially a single primary drying experiment. Further improvement in the proposed optimization framework could be obtained by including the pressure dependency of the choked flow conditions within the formulation of the optimization problem. This could result in an additional reduction of the duration of the primary drying step.

AUTHOR INFORMATION

Corresponding Author

Massimiliano Barolo − *CAPE-Lab − Computer-Aided Process Engineering Laboratory, Department of Industrial Engineering, University of Padova, 35131 Padova, PD, Italy;* orcid.org/0000-0002-8125-5704; Email: max.barolo@unipd.it

Authors

Gabriele Bano − *CAPE-Lab − Computer-Aided Process Engineering Laboratory, Department of Industrial Engineering, University of Padova, 35131 Padova, PD, Italy*

Riccardo De-Luca − *CAPE-Lab − Computer-Aided Process Engineering Laboratory, Department of Industrial Engineering, University of Padova, 35131 Padova, PD, Italy*

Emanuele Tomba − *GSK, 53100 Siena, SI, Italy*

Agnese Marcelli − *GSK, 53100 Siena, SI, Italy*

Fabrizio Bezzo − *CAPE-Lab − Computer-Aided Process Engineering Laboratory, Department of Industrial Engineering, University of Padova, 35131 Padova, PD, Italy;* orcid.org/0000-0003-1561-0584

Complete contact information is available at: https://pubs.acs.org/10.1021/acs.iecr.9b06402

Author Contributions

E.T. and A.M. carried out the experiments and generated the experimental data. G.B., R.D.-L., F.B., and M.B. developed the mathematical model, formulated and solved the optimization problem, and analyzed the experimental results. G.B. coded the model. All authors were involved in the results interpretation. G.B. prepared the manuscript draft with important intellectual input from R.D.-L. and E.T. All authors were involved in revising the manuscript critically for important intellectual content, had full access to the data, and approved the manuscript before it was submitted by the corresponding author.

Funding

This study was conducted under a cooperative research and development agreement between the University of Padova and GlaxoSmithKline Biologicals SA. GSK cofunded this study in the framework of the University of Padova project "Uni-Impresa 2017 − DIGI-LIO − Towards digitalization of the pharmaceutical industry: generation of data with high information content for industrial freeze-drying process optimization".

Notes

The authors declare no competing financial interest.

LIST OF SYMBOLS

a_1, a_2, a_3 = radiation heat-transfer parameters
A_v = cross sectional area of the vial
C_1, C_2, C_3 = heat-transfer parameters
$c_{p,f}$ = specific heat capacity of ice
d_v = vial diameter
J_w = sublimation flux
K_v = heat-transfer coefficient due to conduction
K_r = heat-transfer coefficient due to radiation from upper and lower shelves
L_0 = initial length of the frozen layer
L_d = length of the dried layer
L_f = length of the frozen layer
$\dot{m}_{cd}$ = water flow condensed at the condenser interface
$\dot{m}_s^{tot}$ = total sublimation flow
M_w = molecular weight of water
P_c = total chamber pressure
p^{CM} = capacitance manometer reading of the chamber pressure
$p_{w,c}$ = partial pressure of water vapor in the drying chamber
$p_{w,c}^{exp}$ = experimental value of the water partial pressure
p^{Pirani} = Pirani reading of the chamber pressure
$p_{w,cd}$ = partial pressure of water vapor at the condenser interface
$p_{w,in}$ = partial pressure of water vapor at the sublimation interface
$\dot{Q}_r$ = radiation heat rate from rails
$\dot{Q}_s$ = total heat rate from lower and upper shelves
$\dot{Q}_{sr}$ = heat rate from lower and upper shelves due to radiation
$\dot{Q}_{sv}$ = heat rate from the lower shelf due to conduction
$\dot{Q}_w$ = radiation heat rate from the walls
R_0, R_1, R_2 = mass-transfer parameters
R_g = ideal gas constant
R_p = mass-transfer resistance
$\overline{T}_{cd}$ = mean condenser temperature
T_p = product temperature
$\overline{T}_r$ = mean rail temperature

https://dx.doi.org/10.1021/acs.iecr.9b06402
Ind. Eng. Chem. Res. 2020, 59, 5056−5071

T_{shelf} = shelf temperature
$\overline{T}_w$ = mean wall temperature
$V(y_j)$ = variance of the jth key performance indicator
V_c = chamber volume

Greek Letters

α = parameter of water vapor partial pressure dynamics
ρ_d = density of the dried layer
ρ_f = density of the frozen layer
λ_{N_2} = thermal conductivity of nitrogen
λ_w^v = thermal conductivity of water vapor
σ_{SB} = Boltzmann constant
τ_{dry} = drying time
$\boldsymbol{\theta}$ = vector of model parameters to be estimated

Acronyms

CM = capacitance manometer
KPI = key performance indicator
PRT = pressure rise test
TDLAS = tunable diode laser absorption spectroscopy

REFERENCES

(1) Pikal, M. J. Use of laboratory data in freeze drying process design: heat and mass transfer coefficients and the computer simulation of freeze drying. *PDA J. Pharm. Sci. Technol.* **1985**, *39*, 115−139.
(2) Bjelosevic, M.; Seljak, K. B.; Trstenjak, U.; Logar, M.; Brus, B.; Ahlin Grabnar, P. Aggressive conditions during primary drying as a contemporary approach to optimize freeze-drying cycles of biopharmaceuticals. *Eur. J. Pharm. Sci.* **2018**, *122*, 292−302.
(3) Antelo, L. T.; Passot, S.; Fonseca, F.; Trelea, I. C.; Alonso, A. A. Toward optimal operation conditions of freeze-drying processes via a multilevel approach. *Drying Technol.* **2012**, *30*, 1432−1448.
(4) Patel, S. M.; Doen, T.; Pikal, M. J. Determination of end point of primary drying in freeze-drying process control. *AAPS PharmSciTech* **2010**, *11*, 73−84.
(5) Bellows, R. J.; King, C. J. Freeze-drying of aqueous solutions: Maximum allowable operating temperature. *Cryobiology* **1972**, *9*, 559−561.
(6) Tang, X. C.; Pikal, M. J. Design of freeze-drying processes for pharmaceuticals: practical advice. *Pharm. Res.* **2004**, *21*, 191−200.
(7) Liapis, A. I.; Bruttini, R. Freeze-drying of pharmaceutical crystalline and amorphous solutes in vials: dynamic multi-dimensional models of the primary and secondary drying stages and qualitative features of the moving interface. *Drying Technol.* **1995**, *13*, 43−72.
(8) Mascarenhas, W. J.; Akay, H. U.; Pikal, M. J. A computational model for finite element analysis of the freeze-drying process. *Comput. Methods Appl. Mech. Eng.* **1997**, *148*, 105−124.
(9) Sheehan, P.; Liapis, A. I. Modeling of the primary and secondary drying stages of the freeze drying of pharmaceutical products in vials: Numerical results obtained from the solution of a dynamic and spatially multi-dimensional lyophilization model for different operational policies. *Biotechnol. Bioeng.* **1998**, *60*, 712−728.
(10) Pisano, R.; Fissore, D.; Barresi, A. A. Freeze-drying cycle optimization using model predictive control techniques. *Ind. Eng. Chem. Res.* **2011**, *50*, 7363−7379.
(11) Ramšak, M.; Ravnik, J.; Zadravec, M.; Hriberšk, M.; Iljaž, J. Freeze-drying modeling of vial using BEM. *Engineering Analysis with Boundary Elements* **2017**, *77*, 145−156.
(12) Scutellà, B.; Plana-Fattori, A.; Passot, S.; Bourlès, E.; Fonseca, F.; Flick, D.; Trelea, I. C. 3D mathematical modelling to understand atypical heat transfer observed in vial freeze-drying. *Appl. Thermal Eng.* **2017**, *126*, 226−236.
(13) Millman, M. J.; Liapis, A. I.; Marchello, J. M. An analysis of the lyophilization process using a sorption-sublimation model and various operational policies. *AIChE J.* **1985**, *31*, 1594−1604.
(14) Sadikoglu, H.; Liapis, A. I. Mathematical modelling of the primary and secondary drying stages of bulk solution freeze-drying in trays: Parameter estimation and model discrimination by comparison of theoretical results with experimental data. *Drying Technol.* **1997**, *15*, 791−810.
(15) Velardi, S. A.; Barresi, A. A. Development of simplified models for the freeze-drying process and investigation of the optimal operating conditions. *Chem. Eng. Res. Des.* **2008**, *86*, 9−22.
(16) Fissore, D., Pisano, R., Barresi, A. A. Using mathematical modeling and prior knowledge for QbD in freeze-drying processes. *Quality by Design for Biopharmaceutical Drug Product Development*; Springer, New York, 2015; pp 565−593.
(17) Nail, S. L.; Searles, J. A. Elements of quality by design in development and scale-up of freeze-dried parenterals. *Biopharm Int.* **2008**, *21*, 44−52.
(18) Hardwick, L. M.; Paunicka, C.; Akers, M. J. Critical factors in the design and optimisation of lyophilisation processes. *Innov Pharm. Technol.* **2008**, *26*, 70−74.
(19) Pisano, R.; Fissore, D.; Barresi, A. A.; Brayard, P.; Chouvenc, P.; Woinet, B. Quality by design: optimization of a freeze-drying cycle via design space in case of heterogeneous drying behavior and influence of the freezing protocol. *Pharm. Dev. Technol.* **2013**, *18*, 280−295.
(20) Fissore, D.; Pisano, R.; Barresi, A. A. On the methods based on the Pressure Rise Test for monitoring a freeze-drying process. *Drying Technol.* **2010**, *29*, 73−90.
(21) Fissore, D.; Pisano, R.; Barresi, A. A. Advanced approach to build the design space for the primary drying of a pharmaceutical freeze-drying process. *J. Pharm. Sci.* **2011**, *100*, 4922−4933.
(22) Fissore, D.; Barresi, A. A. Scale-up and process transfer of freeze-drying recipes. *Drying Technol.* **2011a**, *29*, 1673−1684.
(23) Bosca, S.; Barresi, A. A.; Fissore, D. Use of a soft sensor for the fast estimation of dried cake resistance during a freeze-drying cycle. *Int. J. Pharm.* **2013**, *451*, 23−33.
(24) Bosca, S.; Fissore, D.; Demichela, M. Risk-based design of a freeze-drying cycle for pharmaceuticals. *Ind. Eng. Chem. Res.* **2015**, *54*, 12928−12936.
(25) Mortier, S. T. F.; Van Bockstal, P. J.; Corver, J.; Nopens, I.; Gernaey, K. V.; De Beer, T. Uncertainty analysis as essential step in the establishment of the dynamic Design Space of primary drying during freeze-drying. *Eur. J. Pharm. Biopharm.* **2016**, *103*, 71−83.
(26) Pikal, M. J.; Roy, M. L.; Shah, S. Mass and heat transfer in vial freeze-drying of pharmaceuticals: Role of the vial. *J. Pharm. Sci.* **1984**, *73*, 1224−1237.
(27) Vallan, A. A measurement system for lyophilization process monitoring. *2007 IEEE Instrumentation & Measurement Technology Conference, IMTC 2007*; IEEE: Warsaw, 2007; pp 1−5.
(28) Kessler, W. J.; Davis, S. J.; Mulhall, P. A.; Finson, M. L. System for monitoring a drying process. U.S. Patent Application 0208191 A1 A1, Sept 21, 2006.
(29) Kuu, W. Y.; Nail, S. L.; Sacha, G. Rapid determination of vial heat transfer parameters using tunable diode laser absorption spectroscopy (TDLAS) in response to step-changes in pressure set-point during freeze-drying. *J. Pharm. Sci.* **2009**, *98*, 1136−1154.
(30) Schneid, S.; Gieseler, H. Evaluation of a new wireless temperature remote interrogation system (TEMPRIS) to measure product temperature during freeze drying. *AapsPharmscitech.* **2008**, *9*, 729−739.
(31) Pikal, M. J.; Mascarenhas, W. J.; Akay, H. U.; Cardon, S.; Bhugra, C.; Jameel, F.; Rambhatla, S. The nonsteady state modeling of freeze drying: in-process product temperature and moisture content mapping and pharmaceutical product quality applications. *Pharm. Dev. Technol.* **2005**, *10*, 17−32.
(32) Pikal, M. J.; Pande, P.; Bogner, R.; Sane, P.; Mudhivarthi, V.; Sharma, P. Impact of Natural Variations in Freeze-Drying Parameters on Product Temperature History: Application of Quasi Steady-State Heat and Mass Transfer and Simple Statistics. *AAPS PharmSciTech* **2018**, *19*, 2828−2842.
(33) Process Systems Enterprise Ltd. *gPROMS Model Builder*, v 5.1; Process Systems Enterprise Ltd.: London (accessed in 2019).
(34) Johansen, S.; Juselius, K. Maximum likelihood estimation and inference on cointegration—with applications to the demand for money. *Oxf. Bull. Econ. Stat.* **1990**, *52*, 169−210.

https://dx.doi.org/10.1021/acs.iecr.9b06402
Ind. Eng. Chem. Res. 2020, 59, 5056−5071

(35) Scutellà, B.; Trelea, I. C.; Bourlès, E.; Fonseca, F.; Passot, S. Determination of the dried product resistance variability and its influence on the product temperature in pharmaceutical freeze-drying. *Eur. J. Pharm. Biopharm.* **2018**, *128*, 379−388.
(36) Pikal, M. J.; Bogner, R.; Mudhivarthi, V.; Sharma, P.; Sane, P. Freeze-drying process development and scale-up: scale-up of edge vial versus center vial heat transfer coefficients, Kv. *J. Pharm. Sci.* **2016**, *105*, 3333−3343.
(37) Trelea, I. C.; Fonseca, F.; Passot, S.; Flick, D. A binary gas transport model improves the prediction of mass transfer in freeze drying. *Drying Technol.* **2015**, *33*, 1849−1858.
(38) Ganguly, A.; Varma, N.; Sane, P.; Bogner, R.; Pikal, M.; Alexeenko, A. Spatial variation of pressure in the lyophilization product chamber part 1: computational modeling. *AAPS PharmSciTech* **2017**, *18*, 577−585.
(39) Sane, P.; Varma, N.; Ganguly, A.; Pikal, M.; Alexeenko, A.; Bogner, R. H. Spatial variation of pressure in the lyophilization product chamber part 2: experimental measurements and implications for scale-up and batch uniformity. *AAPS PharmSciTech* **2017**, *18*, 369−380.
(40) Scutellà, B.; Passot, S.; Bourlés, E.; Fonseca, F.; Trelea, I. C. How vial geometry variability influences heat transfer and product temperature during freeze-drying. *J. Pharm. Sci.* **2017**, *106*, 770−778.
(41) Goff, J. A.; Gratch, S. Low-pressure properties of water from −160 to 212 ∈F. *Transactions of the American Society of Heating and Ventilating Engineers*; 52nd annual meeting of the American Society of Heating and Ventilating Engineers; New York, 1946; pp 95−122.
(42) Schneid, S.; Gieseler, H. Effect of concentration, vial size, and fill depth, on product resistance of sucrose solution during freeze-drying. *Proceedings of the 6th World Meeting on Pharmaceutics, Biopharmaceutics and Pharmaceutical Technology*; Barcelona, Spain, 2008.
(43) Saltelli, A.; Ratto, M.; Andres, T.; Campolongo, F.; Cariboni, J.; Gatelli, D.; Saisana, M.; Tarantola, S. *Global Sensitivity Analysis: The Primer*; Wiley: Hoboken, NJ, 2008.
(44) Sobol', I. M. Sensitivity estimates for nonlinear mathematical models. *Mathem. Mod.* **1993**, *1*, 407−414.
(45) Sobol', I. M. Global sensitivity indices for nonlinear mathematical models and their Monte Carlo estimates. *Math. Comput. Simul.* **2001**, *55*, 271−280.
(46) Saltelli, A.; Annoni, P.; Azzini, I.; Campolongo, F.; Ratto, M.; Tarantola, S. Variance based sensitivity analysis of model output: design and estimator for the total sensitivity index. *Comput. Phys. Commun.* **2010**, *181*, 259−270.
(47) Van Bockstal, P. J.; Mortier, S. T. F. C.; Corver, J.; Gernay, K. V.; De Beer, T. Global sensitivity analysis as good modelling practices tool for the identification of the most influential process parameters of the primary drying step during freeze-drying. *Eur. J. Pharm. Biopharm.* **2018**, *123*, 108−116.
(48) Scutellà, B.; Trelea, I. C.; Bourlés, E.; Fonseca, F.; Passot, S. Use of a multi-vial mathematical model to design freeze-drying cycles for pharmaceuticals at known risk of failure. *IDS 2018. 21st International Drying Symposium Proceedings*; Editorial UniversitatPolitècnica de València, 2018; pp 315−322.

https://dx.doi.org/10.1021/acs.iecr.9b06402
Ind. Eng. Chem. Res. 2020, 59, 5056−5071